



The modified Beckmann–Kirchhoff scattering theory for rough surface analysis

Hossein Ragheb^{a,*}, Edwin R. Hancock^b

^a*Department of Computer Engineering, Bu-Ali Sina University, P.O. Box 65175-4161, Hamedan, Iran*

^b*Department of Computer Science, University of York, York, YO10 5DD, UK*

Received 2 May 2006; received in revised form 18 September 2006; accepted 2 October 2006

Abstract

This paper focusses on how reflectance models based on scattering theory and reported in the physics literature can be used for making estimates of surface roughness parameters using reflectance measurements obtained with a digital camera. We commence by reviewing the Beckmann–Kirchhoff (B–K) scatter theory, and the recent modification to it by Vernold and Harvey. We show how this model can be used to estimate surface roughness parameters for dielectric surfaces using pixel brightness measurements. Using the roughness parameter measurements we compare the model with reflectance measurements from the CURET database. This comparison shows that the Vernold–Harvey modification of the B–K model gives a better fit to data than the Oren–Nayar model for certain types of rough surface. © 2006 Pattern Recognition Society. Published by Elsevier Ltd. All rights reserved.

Keywords: Rough surface scattering; Physics-based reflectance models; Beckmann model; BRDF measurements; Roughness estimation

1. Introduction

Reflectance modeling is a task of pivotal importance in the analysis of image data. For instance, in computer graphics it is necessary for generating realistic images of scenes [1]. In computer vision, on the other hand, reflectance models form the basis of shape analysis techniques such as shape from shading (SFS) and photometric stereo, and may also be used to estimate the physical properties of materials from passively sensed image data [2]. In this paper we are interested in the reflectance properties of rough surfaces. This is a topic of current importance since recent theories of surface texture have moved away from the naive idea that texture is painted onto the surface. Instead, attempts are being made to understand the formation of texture in terms of surface relief distributions [3,4]. This is a complex problem, since the effect of variable surface roughness is to change the entire reflectance. For instance, a perfectly smooth

surface has purely specular reflectance and hence acts as a mirror by reflecting the light in the incidence plane so that the incidence and reflectance angles are equal. Rough specular surfaces, on the other hand, reflect light into a lobe around the specular direction. As first observed by Lambert, under ideal diffuse reflection, matte surfaces without macroscopic roughness appear equally bright from all viewing directions. For a matte surface, however, the surface appears brighter as the viewer approaches the light-source position. The effect of roughness is also to change the total reflectance, but this effect is weak in most cases and only becomes significant for particular illumination configurations. Of course, at large angles self-shadowing becomes important too, and several authors [5–7] have developed models that account for such an effect.

Roughness is a measure of the statistical variation in the distribution of topographic relief of a surface [8]. The most frequently used statistical parameter for roughness is the root-mean-square (RMS) height σ [8]. Although there is conflicting evidence, for ideal surfaces the height distribution is frequently assumed to be Gaussian [9], and this can be justified if the height distribution is the result of a single

* Corresponding author. Fax: +98 8118257400.

E-mail addresses: ragheb@basu.ac.ir (H. Ragheb), erh@cs.york.ac.uk (E.R. Hancock).

random process. Unfortunately, the specification of a height distribution, and hence RMS roughness, is insufficient to discriminate between surfaces with different roughness length scales. Such surfaces may, however, be distinguished on the basis of their correlation functions [10]. It is frequently assumed that the correlation function is Gaussian. However, in practice, the exponential correlation function is sometimes found to give a better fit to the measured surface data [9]. Length and height effects may be jointly characterized using the RMS slope parameter, which is a measure of the difference between the measured heights of adjacent points divided by the data sampling interval. These roughness parameters can either be estimated directly from surface-profile measurements, or they can be calculated from a scattering measurement using a theoretical reflectance model [8].

There have been a number of attempts to model rough surface reflectance. These models can be divided into those that model the effect of roughness on the specular reflectance component and those that attempt to account for the diffuse reflectance component. Turning our attention first to the specular component, the Torrance–Sparrow model [11] uses roughness to account for the shape of the specular lobe. The model is based on geometrical optics, and is hence applicable when the surface irregularities are much larger than the wavelength of the incident radiation, and has been shown by Nayar et al. [12] to be a more elaborate version of the earlier Beckmann model [10]. Roughness effects have also been incorporated into the diffuse reflectance model developed by Oren and Nayar [13]. This model assumes that the surface is composed of V-shaped cavities that reflect light in a Lambertian manner. It is the angular distribution of the cavity walls that gives rise to departures from Lambert's law. A major drawback of the Oren–Nayar (O–N) model is that, because it relies on the assumption of surface isotropy, the cavities associated with roughness have no preferred direction and isotropic cavitated surfaces cannot exist [2]. To overcome this problem van Ginneken et al. have recently developed a model that can be used to predict reflectance from isotropic rough surfaces that have both specular and diffuse components [2]. The parameters of their model are the surface roughness measured in terms of the RMS slope, the albedo, and the balance between the diffuse and specular components. Finally, Wolff et al. [14] have attempted to incorporate more physics into the modeling process by using the Fresnel term to model subsurface refractive attenuation.

Although some of these papers are motivated by the need to incorporate more principled reflectance models, they fall short of developing purely physics-based models that account for directly measurable roughness parameters. To address this omission, in this paper, we provide an analysis of some physically based models for the scattering of light from rough surfaces. One of the most straightforward approaches is to develop a model based on geometrical optics. Underlying the approach is the assumption that the scattering surface consists of planar facets having lateral dimensions that

are large compared to the wavelength of the incident light and which reflect like plane mirrors [15]. Each facet has a surface normal and there will be a statistical distribution of the directions of the surface normals. Thus, according to geometrical optics, scattering from a rough surface consists of summing the contributions from each tilted facet of the surface. In order to analyze a surface using this approach, one needs a characterization of the surface. This can be either a model of the shape and angular distribution of the surface facets or an equivalent statistical characterization. For instance, Beckmann [10] developed a Markov chain model to account for the surface statistics. However, it is difficult to develop statistical models that give realistic predictions.

These problems were circumvented by Beckmann [16] who used the scalar theory of wave scattering. Whereas geometrical optics involves ray-tracing and is diffraction limited, scattering theory models the interactions between the wave and the surface. The scalar version of wave scattering theory accounts only for the distribution of energy, and does not account for more complex effects such as polarization. Scalar wave scattering models have been applied both to surfaces whose roughness (in practice, the typical dimension of a local flat area) is much less than the wavelength of light [17–19] and also to those whose roughness is much greater than the wavelength of light [18,20]. The starting point for the scalar wave theory treatment of scattering from rough surfaces is the Helmholtz–Kirchhoff diffraction integral [15]. To overcome some problems involved in solving this integral, an approximation known as the Kirchhoff boundary condition is made. The Beckmann formulation of the scalar Kirchhoff theory (referred to here as the Beckmann–Kirchhoff or B–K theory) is the most widely used in the study of wave scattering from rough surfaces. Despite its widespread use, the B–K theory is based on a paraxial (small-angle) assumption that limits its ability to accurately account for both wide-angle scattering and large angles of incidence [21]. Recently, Vernold and Harvey [22] have modified the B–K theory to overcome this limitation. Their modification involves replacing the geometrical form factor of the B–K theory by a simpler Lambertian form. This extends the utility of the theory to large angles of both incidence and scatter. In fact, Harvey et al. [21] have critically analyzed this problem and have developed a linear system approach to wide-angle scalar diffraction theory. It should be noted that the B–K theory is applicable to both dielectric and metallic surfaces. However, here we confine our attention to the use of the theory to analyze dielectric surfaces with different scales of roughness. However, specific models of wave scattering from machined metal surfaces have been developed by Bennett and Porteus [17] and by Torrance [23]. Both of these models have been developed from the Davies theory [18] of electromagnetic wave reflection from rough surfaces.

Although the Kirchhoff integral is well known in physical optics, the B–K approximation has not received significant attention in computer vision or image processing. There has,

however, been some interest in the use of the B–K theory in the graphics community. For instance, it has been used by He et al. [24] to develop a quite elaborate reflectance model which accounts for both specular and diffuse reflectance. The specular component depends on the effective roughness σ , while the directional dependence of the diffuse component is governed by both the correlation function of the surface and σ . An important feature of the model is that it incorporates a detailed description of the effects of surface height and slope by averaging the Kirchhoff integral.

Our aim in this paper is to investigate whether the B–K wave scattering theory can be used for rough surface analysis using reflectance measurements obtained with a digital camera. We commence by reviewing the main wave scattering models for light scattering from rough surfaces, and state the conditions under which they apply. We reformulate the wave scattering models in a manner so that they can be applied to brightness measurements provided by digital images. We then show how the models may be used to make estimates of surface roughness parameters using information extracted from digital images of planar surface samples. Specifically, we show how the B–K theory can be used to make roughness estimates using just two reflectance measurements obtained using a digital camera. Finally, we compare the predictions of a number of alternative models against the bidirectional reflectance distribution function (BRDF) measurements from the CURET database. This shows that, of the alternatives studied, the Vernold–Harvey (V–H) modification of the B–K model gives the agreement with experimental data for a range of samples.

The outline of the remainder of this paper is as follows. In Section 2 we briefly summarize some of the physics of image formation and provide definitions of the radiometric quantities used in the paper. Section 3 focusses on the B–K scattering theory and modifications to it. In Section 4 we describe how the models outlined in Section 3 can be used to develop methods for estimating rough surface parameters. Section 5 describes how we can simplify the model for a specific illumination configuration and provides experiments on real-world data. Finally, Section 6 offers conclusions and suggests directions for future investigation.

2. Imaging geometry

The geometry of light scattering and image formation is illustrated in Fig. 1. Using this imaging geometry, Horn [25] has derived a relationship between surface radiance and image irradiance. We consider a surface illuminated by a parallel beam of light of known wavelength λ and viewed by a camera which is sufficiently distant from the surface so that parallax effects may be ignored. The direction \vec{L} , shown in Fig. 1, stands for the direction pointing from the illuminated point p on the surface towards the light-source position. This is a definition used in computer vision, while in optical physics the opposite direction ($-\vec{L}$) is used instead. However, both methods give identical results since the combination of zenith and azimuth angles completely define the illumination configuration. We consider the interaction of the light with the surface at a location p where the surface normal is \vec{N} . The direction of the optical axis of the camera, or viewing direction, is denoted by \vec{V} . The incident light has zenith angle θ_i and azimuth angle ϕ_i with respect to the surface normal, while the zenith and azimuth angles of the viewing (scattering) direction with respect to the surface normal are θ_s and ϕ_s (ϕ_i and ϕ_s are not shown in Fig. 1).

The radiance of the incident light beam at the location on the surface is $\mathcal{L}_i(\theta_i, \phi_i)$ and the outgoing radiance is $\mathcal{L}_o(\theta_s, \phi_s)$. Suppose that the camera lens has diameter D , and that the image plane is at a distance Z_2 behind the lens. Further suppose that the location p with area dS on the surface (with area S) is imaged by a sensor element u of area dS' , and that the angle between the sensor element and the axis of the camera is α_u . Based on the conservation of radiant flux, the irradiance at the sensor element [25] is $E(\theta_i, \phi_i, \theta_s, \phi_s) = \mathcal{L}_o(\theta_s, \phi_s)(\pi/4)(D/Z_2)^2 \cos^4 \alpha_u$. When the image covers only a narrow angle of the scene and the point p is close to the optical axis, one can assume that $\cos \alpha_u = 1$. Hence, we can write $E(\theta_i, \phi_i, \theta_s, \phi_s) = K_u \mathcal{L}_o(\theta_s, \phi_s)$ where $K_u = (\pi/4)(D/Z_2)^2$, and as a result the brightness of the pixels in the image is proportional to the radiance from the corresponding surface location. To satisfy these assumptions, in practice we experiment with objects whose dimensions are comparable with the

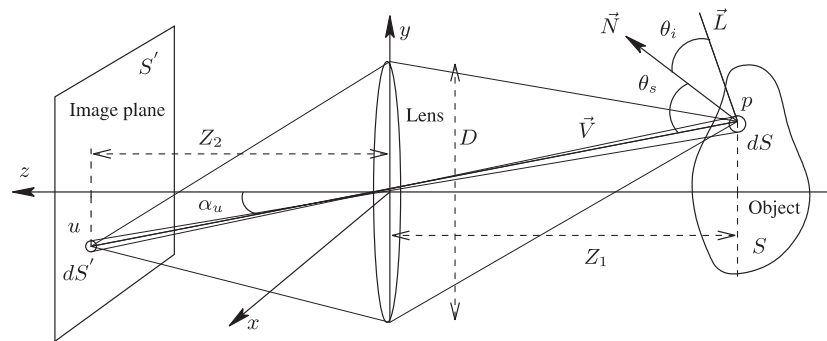


Fig. 1. The imaging geometry used to relate the image irradiance to the surface radiance. The symbols are described in the text. Angles are exaggerated to facilitate visualization.

diameter of the camera lens. We also point the camera optical axis towards the center of the object, which is at large distance from the camera. Hence, in this paper, we are going to apply the small-angle assumption to relate the scene radiance to the focal plane irradiance. By dividing all pixel brightness values by the largest brightest value in the image, the effects of lens transmission, etc. are normalized out.

In Section 5.3 we compare the predictions of wave scattering theory with BRDF measurements from the CURET database [24,26–28]. Suppose that $f(\theta_i, \phi_i, \theta_s, \phi_s)$ is the BRDF measurement for the surface with the light source and viewing directions as defined above, then we can write $dE(\theta_i, \phi_i, \theta_s, \phi_s) \propto f(\theta_i, \phi_i, \theta_s, \phi_s) \mathcal{L}_i(\theta_i, \phi_i) \cos(\theta_i) d\omega$ where $d\omega$ is the solid angle of the source subtended at the surface. If the source solid angle $d\omega$ is small and constant, then it drops out on integration and $E(\theta_i, \phi_i, \theta_s, \phi_s) \propto f(\theta_i, \phi_i, \theta_s, \phi_s) \mathcal{L}_i(\theta_i, \phi_i) \cos(\theta_i)$. Of course, this is a very simplistic model of the image formation process. In practice, we work with a digital camera with CCD elements. As a result the measured pixel brightness is the result of transmission through the camera lens and a monotonic mapping of the radiance to the relevant sensor element by the electronic circuitry of the camera. Accurate determination of the surface radiance \mathcal{L}_o or equivalently the radiant intensity requires careful calibration of the camera. As noted above, in our experiments we do not attempt to calibrate the camera, but instead we normalize the pixel brightness values by dividing them by the maximum brightness value for each image.

In Fig. 2 we show the scattering geometry on the tangent plane to the imaged surface. Here, we align the local coordinate system (X_0, Y_0, Z_0) so that the projection of \vec{L} onto the tangent-plane points in the direction of the negative X_0 -axis. Hence, $\phi_i = \pi$ for all scattering geometries. There are three special geometries that will be of interest in this paper. The first of these is the retroscattering (retroreflection) case where \vec{L} and \vec{V} are identical, i.e. $\theta_i = \theta_s = \theta$ and $\phi_s = \pi$. The second case is that of the specular direction where \vec{V} , \vec{L} , and the surface normal are in the same plane, $\theta_i = \theta_s$ and $\phi_s = 0$. The third case is when \vec{L} is off-normal while \vec{V} is normal to

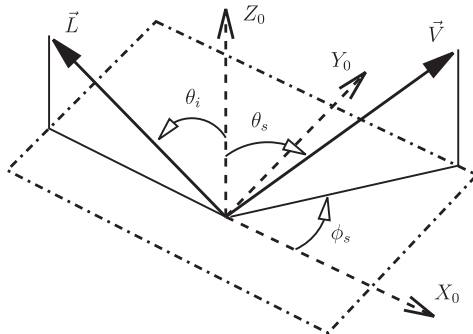


Fig. 2. Scattering geometry on the sample tangent-plane coordinate system: the incident light propagates in the direction $-\vec{L}$, while the direction for the scattered light is \vec{V} .

the tangent plane, i.e. $\theta_i \neq 0, \theta_s = 0$ and $\phi_s = 0$. In practice, we consider pixels close to the center of the digital images.

It is straightforward to find the zenith angles θ_i and θ_s , i.e. $\theta_i = \cos^{-1}(\vec{N} \cdot \vec{L})$ and $\theta_s = \cos^{-1}(\vec{N} \cdot \vec{V})$. The azimuth angle ϕ_s can also be found by computing the angle between the projections of the vectors \vec{L} and \vec{V} on the local tangent plane. Specifically, $\phi_s = \pi - \cos^{-1}[(\vec{L}_p \cdot \vec{V}_p)/(\|\vec{L}_p\| \|\vec{V}_p\|)]$ where the projected vectors are given by $\vec{L}_p = \vec{N} \times \vec{L} \times \vec{N}$ and $\vec{V}_p = \vec{N} \times \vec{V} \times \vec{N}$. Note that here $\phi_i = \pi$ and also the values of ϕ_s obtained using these equations agree with the geometry of Fig. 2.

3. B–K scattering theory

The B–K theory attempts to account for the wave interactions of light with opaque rough surfaces. The starting point is Kirchhoff’s integral which gives the scattered light-field amplitude. Beckmann’s contribution was to show how to apply the theory to rough surfaces, and how to obtain simplifications to the Kirchhoff integral under different roughness conditions. The details of the theory are comprehensively described in the monographs of Beckmann and Spizzichino [10], and by Ogilvy [9].

3.1. Basic theory

Hence, in this section we consider the B–K theory for light scattering from rough surfaces. Commencing from the Helmholtz–Kirchhoff diffraction integral, and by requiring that the surface has both a Gaussian surface height distribution and a Gaussian surface correlation function, the B–K theory can be used to compute the mean scattered power $P(\theta_i, \phi_i, \theta_s, \phi_s) = \langle \rho \rho^* \rangle$, where the scattering coefficient $\rho = \mathcal{E}_2 / \mathcal{E}_{20}$ is the ratio of the scattered field \mathcal{E}_2 from the rough surface to the corresponding reflected field \mathcal{E}_{20} from a smooth, perfectly reflecting plane of the same material and dimensions illuminated by an incident wave that is polarized parallel to the plane of incidence with the same incidence geometry [10]. It has been widely assumed that the mean scattered power $\langle \rho \rho^* \rangle$ (the mean of the squared modulus of the scattered electric field) is proportional to the mean optical intensity or the measured irradiance [16, p. 62]. The reason for this is that the B–K theory is based on a small-angle approximation. Since in the paraxial region where both θ_i and θ_s are small, $\cos \theta_i \approx 1$ and $\cos \theta_s \approx 1$, and so radiance and intensity are approximately equivalent [21]. However, alternative radiometric quantities may also be computed using the Helmholtz–Kirchhoff integral as a starting point [9,12,29–31].

The B–K model has two main physical parameters. The first of these is the RMS height deviation of the topographic surface features about the mean surface level which is denoted by σ . The height values are generally measured at equally spaced digitized data points. When the roughness is defined in one dimension only, the height variations Δz of

the surface are assumed to follow the Gaussian distribution function $W(\Delta z) = (1/\sigma\sqrt{2}) \exp(-\Delta z^2/2\sigma^2)$. The second parameter is the correlation length T which is defined in terms of the surface correlation function $C(\tau)$ so that $T^2 = 2 \int_0^\infty \tau C(\tau) d\tau$. The correlation function characterizes the random nature of a surface profile and the relative spacing of peaks and valleys. For a purely random surface, $C(\tau)$ decreases monotonically from its maximum value $C(0) = 1$ to $C(\infty) = 0$. Specifically, the correlation length is the lag length at which the Gaussian correlation function $C(\tau) = \exp(-\tau^2/T^2)$ drops to $1/e$. Similarly, for the exponential correlation function $C(\tau) = \exp(-|\tau|/T)$ it follows that $C(T) = 1/e$. For a rough surface the relation between z , σ , and T are given by Marx and Vorburger [32]. In terms of the digitized heights, the RMS roughness is found using $\sigma^2 = (1/N) \sum_{k=1}^N z_k^2$, where z_k are the heights relative to a mean line fitted to the measured data by a least-square fit procedure. Hence, the function $C(\tau)$ can be approximately represented by the coefficients C_j computed from the digitized heights z_k so that $C_j[1/\sigma^2(N-j)] = \sum_{k=1}^{N-j} z_k z_{j+k}$ where $j = 0, 1, \dots$ [32]. Each value of C_j constituting an unbiased estimator, which has a factor N instead of $N-j$ in the denominator, is sometimes preferred since it shows no instabilities as the values of j approach N [32]. Depending on whether $C(\tau)$ follows the Gaussian, the exponential, or any other standard form of correlation function, T can easily be computed from $C(\tau)$. However, if $C(\tau)$ is not governed by one of the standard correlation functions, then it may not be a straightforward task to find T using $C(\tau)$. This study may be extended to the case where roughness is studied in two dimensions on isotropic surfaces [10]. Here, the normal distribution of height variation (with mean zero, standard deviation σ , and correlation function $C(\tau)$) is $W(\Delta z_1, \Delta z_2) = [1/2\pi\sigma^2\sqrt{(1-C^2)}] \exp[-(\Delta z_1^2 - 2C\Delta z_1\Delta z_2 + \Delta z_2^2)/2\sigma^2(1-C^2)]$. Note that the expressions for $C(\tau)$ are identical to those described in the case of roughness in one dimension. In this paper we study surface roughness in two dimensions, and hence all the equations used later on in the paper correspond to such surfaces. According to the B-K model [10], for a surface that is smooth or of intermediate roughness in the tangent-plane coordinate system the mean scattered power is given by

$$P(\theta_i, \phi_i = \pi, \theta_s, \phi_s) = \rho_0^2 e^{-g(\theta_i, \theta_s)} + \mathcal{D}(\theta_i, \phi_i, \theta_s, \phi_s), \quad (1)$$

where the first term is the coherent scattering component in the specular direction and the second term is the incoherent component due to diffuse scattering. The specular term is a product of two terms. The first of these is the magnitude specular reflectance ρ_0 which is a very sharp function of θ_i and θ_s . The magnitude ρ_0 is nearly zero for all scattering directions except a very narrow range around the specular direction. The second term is an exponential function of the quantity $g(\theta_i, \theta_s) = \sigma^2 v_z^2(\theta_i, \theta_s)$ where $v_z(\theta_i, \theta_s) = -k(\cos \theta_i + \cos \theta_s)$ and $k = 2\pi/\lambda$, and this controls the

relative magnitude of the specular component. When the correlation function is *Gaussian*, with the geometry shown in Fig. 2 on the tangent plane (the incident beam has azimuth angle $\phi_i = \pi$), according to Ref. [10] the diffuse component is

$$\mathcal{D}(\theta_i, \phi_i = \pi, \theta_s, \phi_s) = \left(\frac{\pi T^2}{A} \right) \frac{F^2(\theta_i, \theta_s, \phi_s)}{\exp[g(\theta_i, \theta_s)]} \times \sum_{n=1}^{\infty} \left\{ \frac{g^n(\theta_i, \theta_s)}{n!n} \exp \left[\frac{-T^2}{4n} v_{xy}^2(\theta_i, \theta_s, \phi_s) \right] \right\}, \quad (2)$$

where $v_x(\theta_i, \theta_s, \phi_s) = k(\sin \theta_i - \sin \theta_s \cos \phi_s)$, $v_y(\theta_s, \phi_s) = -k(\sin \theta_s \sin \phi_s)$, and $v_{xy}^2(\theta_i, \theta_s, \phi_s) = v_x^2(\theta_i, \theta_s, \phi_s) + v_y^2(\theta_s, \phi_s)$. The scattering takes place from a rectangular surface patch of area $A = 4XY$ whose dimensions are $2X$ and $2Y$ in the X_0 and Y_0 directions. Using this definition we have $\rho_0 = [\sin(v_x X)/(v_x X)][\sin(v_y Y)/(v_y Y)]$. For scattering directions which are very close to the specular direction we have $\theta_i \rightarrow \theta_s$ and $\phi_s \rightarrow 0$, and so $v_x \rightarrow 0$ and $v_y \rightarrow 0$ which gives $\rho_0 = 1$. In practice, for all real-world materials, specifically for dielectrics, we have $\rho_0 < 1$. The quantity F appearing in the second term is the *geometric factor*, and as we will see in Section 3.2, its choice is of critical importance to the model. It is interesting to note that in the specular direction when $\theta_i = \theta_s$ and $\phi_r = 0$, then $v_{xy}^2(\theta_i, \theta_s, \phi_s) = 0$ and the diffuse component $\mathcal{D} \propto g(\theta_i, \theta_s) \exp[-g(\theta_i, \theta_s)]$ is controlled by the quantity g too.

The quantity $g(\theta_i, \theta_s)$ plays another important role, since it has been used in the literature to divide surfaces into three broad categories. These are (a) slightly rough ($g(\theta_i, \theta_s) \ll 1$), (b) moderately rough ($g(\theta_i, \theta_s) \simeq 1$), and (c) very-rough ($g(\theta_i, \theta_s) \gg 1$) surfaces. When the correlation function is *Gaussian*, then two of these cases lead to interesting simplifications of the B-K model. When the surface is slightly rough ($g(\theta_i, \theta_s) \ll 1$) then only the first term in the series of Eq. (2) needs to be considered and the diffuse component becomes [10]

$$\mathcal{D}(\theta_i, \phi_i = \pi, \theta_s, \phi_s) = \left(\frac{\pi T^2}{A} \right) g(\theta_i, \theta_s) F^2(\theta_i, \theta_s, \phi_s) \times \exp \left[-g(\theta_i, \theta_s) - \frac{T^2}{4} v_{xy}^2(\theta_i, \theta_s, \phi_s) \right]. \quad (3)$$

The second interesting case for the Gaussian correlation function arises when the surface is very rough ($g(\theta_i, \theta_s) \gg 1$). Under these conditions the expression for the diffuse component of the mean scattered power becomes [10]

$$\mathcal{D}(\theta_i, \phi_i = \pi, \theta_s, \phi_s) = \left(\frac{\pi T^2}{A\sigma^2} \right) \frac{F^2(\theta_i, \theta_s, \phi_s)}{v_z^2(\theta_i, \theta_s)} \times \exp \left[\frac{-T^2 v_{xy}^2(\theta_i, \theta_s, \phi_s)}{4\sigma^2 v_z^2(\theta_i, \theta_s)} \right]. \quad (4)$$

For different surface correlation functions there are different scattering behaviors. If the correlation function is *exponential* rather than *Gaussian*, then the diffuse

component of the mean scattered power for very-rough surfaces ($g(\theta_i, \theta_s) \gg 1$) is given by [16]

$$\mathcal{D}(\theta_i, \phi_i = \pi, \theta_s, \phi_s) = \left(\frac{2\pi T^2}{A\sigma^2} \right) \times \frac{F^2(\theta_i, \theta_s, \phi_s)}{v_z^2(\theta_i, \theta_s)[1 + T^2 v_{xy}^2(\theta_i, \theta_s, \phi_s)/\sigma^2 v_z^2(\theta_i, \theta_s)]^{3/2}}. \quad (5)$$

3.2. Modified theory

In Eq. (2), the geometrical factor F derived by Beckmann (F_{Beck}) is given by [10]

$$F_{Beck}(\theta_i, \theta_s, \phi_s) = \frac{1 + \cos \theta_i \cos \theta_s - \sin \theta_i \sin \theta_s \cos \phi_s}{\cos \theta_i (\cos \theta_i + \cos \theta_s)}. \quad (6)$$

Unfortunately, as highlighted by several authors [22,33], this choice fails to reliably predict the scattering behavior at large angles of incidence and scattering. Specifically, Beckmann and Spizzichino [10] have claimed that for rough reflective surfaces, it is the local surface normal direction that is of primary importance in determining the geometrical factor F . They have indicated that the local surface normal at each point on a rough surface varies as the surface is traversed, and does not coincide with the mean surface normal. Although Vernold and Harvey [22] agree with the observation that the local and mean surface normals do not coincide, they do not agree that a new obliqueness factor is needed to account for the difference in direction. Instead, they claim that it is sufficiently accurate to use the mean surface normal when modeling rough surfaces, under conditions where the wavelength of the incident light is much larger than the spatial scales (heights) under study. Hence, Vernold and Harvey [22] use the geometrical factor $F_{VH}^2 = \cos(\theta_i)$ that is Lambertian in form and depends only on the cosine of the incidence angle. This modification gives reasonable experimental agreement with scattering data for rough surfaces at large angles of incidence and large scattering angles. Note that the modification is not based on a physical model. Instead, it relies on empirical and phenomenological arguments. However, this does not diminish our pragmatic interest in the modified B–K model since it includes some effects (corresponding to non-paraxial angles) which are not included in the original B–K model.

There is considerable debate about the meaning and proper use of the geometrical (inclination) factor F [30]. While we use F_{VH} and F_{Beck} in our experiments, a variety of forms of F have been used in the wave scattering literature. For instance, based on boundary condition considerations Ogilvy [9] argues for the factor $F_{Ogil} = F_{Beck} \cos(\theta_i)$. Ogilvy also stresses that F is independent of the choice of total or scattered field within the B–K integrand [9]. Nieto-Vesperinas and Garcia [29,30] have shown that the factor used by Kirchhoff is related to that of Beckmann by the

formula $F_{Kirch} = F_{Beck} \cos(\theta_i)/\cos(\theta_s)$, and note that a factor $\cos(\theta_s)/\cos(\theta_i)$ is necessary to ensure energy normalization and to prevent the predictions of the B–K theory from becoming infinite when the outgoing light direction grazes the surface.

3.3. Application of theory to digital images

In this paper we use the B–K model to compute surface radiance and to compare the predictions with measured pixel brightness values obtained using a digital camera. The experimental procedure is somewhat different from that adopted in the physical optics literature where the models that we have investigated were originally reported. However, digital cameras have been successfully used in the computer vision literature to make radiometric measurements. For instance, Dana et al. [28] have performed camera calibration using pixel gain and offset values to make radiance estimates. In order to make comparison with the predictions of the Beckmann model we adopt a very simple calibration method and normalize the pixel brightness by applying a single gain value across each image.

However, it is important to note that the radiometric meaning of the scattering calculations performed by Beckmann is the subject of some disagreement in the literature. Beckmann uses the Kirchhoff theory to compute the mean scattered power $P(\theta_i, \phi_i = \pi, \theta_s, \phi_s)$. Ogilvy [9] has reformulated the B–K model and computes the overall scattered intensity $\langle I \rangle$ which is proportional to the mean optical intensity. With the imaging geometry shown in Fig. 1 the scattered intensity is given by $I = \mathcal{L}_o \cos \theta_s dS$, and hence $I \propto E \cos \theta_s$. Harvey et al. [21] have returned to the original formulation of Beckmann, and have shown that the quantity computed by Beckmann is proportional to the diffracted scattered radiance. Specifically, they have shown that while the experimental data collected (using a scattering instrument) by O'Donnell and Mendez [33] are scattered intensities, the predictions from the B–K theory are a better representation of the scattered radiance.

Here, we follow Harvey et al. [21] and interpret Beckmann's result as diffracted scattered radiance rather than scattered intensity. However, it is worth mentioning that if one follows Ogilvy [9], rather than Harvey et al., then all of Ogilvy's expressions for scattered intensity will need to be divided by a further factor of $\cos \theta_s$.

Similarly, to find scattered intensity from scattered radiance, one should multiply the scattered radiance by the cosine of the scattered angle and integrate over the illuminated area on the scattering surface [21]. Hence, in this paper, the predicted pixel brightness resulting from the specular component is $E_s(\theta_i, \phi_i = \pi, \theta_s, \phi_s) = K \rho_0 \exp(-[(2\pi/\lambda)(\cos \theta_i + \cos \theta_s)]^2)$, that is attributable to the diffuse component is $E_d(\theta_i, \phi_i = \pi, \theta_s, \phi_s) = K \mathcal{D}(\theta_i, \phi_i = \pi, \theta_s, \phi_s)$, and that resulting from the total radiance is $E(\theta_i, \phi_i = \pi, \theta_s, \phi_s) = K P(\theta_i, \phi_i = \pi, \theta_s, \phi_s)$, where K is the image gain.

We have not attempted to directly calibrate the camera in our work. This is a difficult task, and requires override of automatic camera settings and a calibrated light source. Instead, we have normalized the pixel brightness values and used relative brightness measurements.

3.4. Retroscattering

To gain some insight into the reflectance models, we focus in detail on the case of retroscattering (generally taken to be the case where the angle of scattering is the negative of the angle of incidence) or retroreflection, where the viewing and light-source directions are the same. This is not an ideal configuration for the perception of relief because of the lack of shadows. However, it does provide a route by which we can utilize the light scattering theory to assist in recovering more accurate surface shape from shading information [34]. The reason for this is that the geometry of retroscattering provides us with significant simplifications of the model, since \vec{L} and \vec{V} become identical.

When $\vec{L}=\vec{V}$, then $\theta_i=\theta_s=\theta$ and $\phi_s=\pi$. In physical optics, it is customary to have $\theta_i=\theta_s$ for specular reflection and $\theta_i=-\theta_s$ for retroscattering geometry. However, when two azimuth angles ϕ_i and ϕ_s are also specified (on the tangent-plane coordinate system), the exact incidence and reflectance vector configurations are completely specified. Hence, there is no need to sign the zenith angles θ_i and θ_s . Under these conditions $v_{xy}(\theta, \theta, \pi)=2k \sin \theta$, $v_z(\theta, \theta)=-2k \cos \theta$, and $F_{Beck}(\theta, \theta, \pi)=1/\cos^2 \theta$. From Eq. (4), when the correlation function is Gaussian, then the diffuse component of the pixel brightness predicted by the B–K model in the retroscattering configuration, i.e. $E_d(\theta_i=\theta, \phi_i=\pi, \theta_s=\theta, \phi_s=\pi)$, is

$$\hat{E}_d^{Beck-Gauss-vr}(\theta)=(K/\cos^6 \theta) \exp[-T^2 \tan^2 \theta/(4\sigma^2)]. \quad (7)$$

The simplified equation for surfaces with an exponential correlation function (Eq. (5)) is

$$\hat{E}_d^{Beck-Exp-vr}(\theta)=K/\{\cos^6 \theta[1+(T/\sigma)^2 \tan^2 \theta]^{3/2}\}. \quad (8)$$

The difference between the simplified radiance functions appearing in Eqs. (7) and (8) is that in the case of the Gaussian correlation function the $1/\cos^6 \theta$ dependence is modified by an exponential function of $\tan^2 \theta$, while in the case of the exponential correlation function the modifying factor is algebraic. The $1/\cos^6 \theta$ approaches infinity as $\theta \rightarrow \pi/2$. In the case of the Gaussian correlation function this behavior is canceled by the exponential function of $\tan^2 \theta$ and the radiance tends to zero as θ approaches $\pi/2$. In the case of the exponential correlation function, the radiance approaches infinity at $\pi/2$, since the algebraic function of $\tan^2 \theta$ does not cancel the infinite behavior of the $1/\cos^6 \theta$ term. Hence, the exponential correlation function results in a physically unrealistic behavior of Eq. (8).

It is also interesting to consider the behavior of the simplified radiance function when the V–H modification to the

B–K model is made. For very rough surfaces with a Gaussian correlation function, and simplified to the case of retroscattering, we have

$$\hat{E}_d^{VH-Gauss-vr}(\theta)=(K/\cos \theta) \exp[-T^2 \tan^2 \theta/(4\sigma^2)]. \quad (9)$$

While the corresponding result for surfaces with an exponential correlation function is

$$\hat{E}_d^{VH-Exp-vr}(\theta)=K/\{\cos \theta[1+(T/\sigma)^2 \tan^2 \theta]^{3/2}\}. \quad (10)$$

Hence, the $1/\cos^6 \theta$ behavior of the original B–K model (Eqs. (7) and (8)) is replaced by a slower $1/\cos \theta$ behavior. Figs. 3 and 4 illustrate the effect of this different behavior for very-rough surfaces. The different curves in each subfigure plot the normalized radiance as a function of the incidence angle for different values of σ/T . The dashed curve in each plot is the prediction of Lambert’s cosine law. Fig. 3 is for the original B–K model (Eqs. (7) and (8)), while Fig. 4 is for the modified B–K model of V–H (Eqs. (9) and (10)). In each figure, subfigure (a) is for the case of a Gaussian correlation function, whereas subfigure (b) is for the exponential correlation function. Fig. 3 demonstrates that the original B–K model diverges significantly from the Lambertian curve for large angles of incidence. Here, in the case of the Gaussian correlation function the normalized radiance peaks at large scatter angles for large values of m because of the $1/\cos^6 \theta$ term. In the case of the exponential correlation function the behavior is infinite at large scatter angles because of the discontinuity of the first derivative of this function at the origin. Fig. 4, on the other hand, shows that the V–H modification to the B–K model does not exhibit these problems. From the different curves in both figures it is also clear that the larger the surface roughness σ with respect to correlation length T , the higher the normalized radiance. For instance, in Figs. 4(a) and (b) for $\sigma/T=0.71$ and 1.8, the brightening effects occur because of the large values of the roughness parameter.

Finally, we consider the behavior of the modified B–K model for slightly rough surfaces with a Gaussian correlation function. When we apply Eq. (3) to the case of retroscattering the predicted image irradiance is

$$\hat{E}_d^{VH-Gauss-sr}(\theta)=K \cos^3(\theta) \exp\{-(2\pi/\lambda)^2([T \sin(\theta)]^2 + [2\sigma \cos(\theta)]^2)\}. \quad (11)$$

It is important to note that in contrast to rough surfaces (Eqs. (7)–(10)), in the case of slightly rough surfaces there is a dependence on the wavelength λ . To our knowledge, there is no closed-form simplification of the B–K model for scattering from slightly rough surfaces with an exponential correlation function.

3.5. Limits of validity

The B–K theory does not account for multiple scattering, which occurs in the cavities of the surface and is important

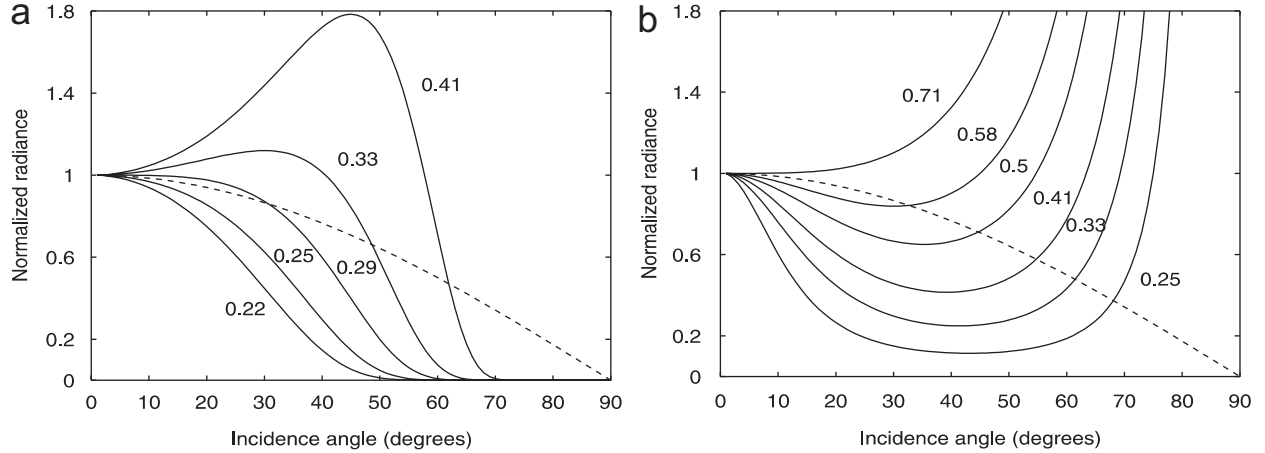


Fig. 3. Normalized radiance using the original B–K model ($F = F_{Beck}$) with a Gaussian (a) or an exponential (b) correlation function versus θ_i for several values of $m = \sigma/T$.

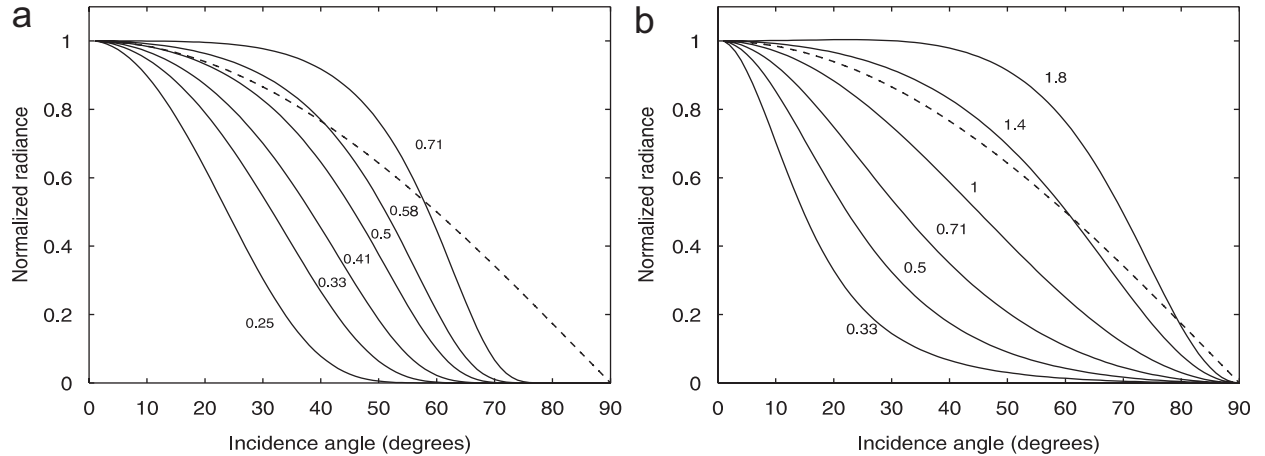


Fig. 4. Plots (as described in Fig. 3 and in the text) for the modified B–K model ($F = F_{VH}$).

for large values of the slope σ/T . When multiple scattering occurs, energy is not transferred directly from the incident wave into the scattered wave, but instead becomes “trapped” for a limited time within the hills and troughs of the rough surface [9]. Hence, the B–K theory underestimates the scattered intensity. Recently, Caron et al. [35] have attempted to model this effect using the energy conservation rate. This is the ratio of the scattered energy to the incident energy, i.e. $\xi_K = \varepsilon_{sc}/\varepsilon_{inc}$. At normal incidence and for $g \gg 1$ and when $0 \leq \theta_s \leq \pi/2$, then $\xi_K = 1 - \exp(-T^2/4\sigma^2)$. Hence, ξ_K is small if the slope is large, while it is large when the slope is low. This quantity also accounts for missing energy because of multiple scattering. This interpretation results from the fact that when the scattering process is integrated over the range $0 \leq \theta_s \leq \pi$ then $\xi_K = 1$ [35].

A second limitation of the B–K theory identified by Caron et al. is that for rough surfaces under oblique incidence there are problems because of surface self-shadowing, caused by

rough protrusions. To address this problem, they have introduced a limit θ_K for angles of incidence less than which the predictions of the B–K model are valid. Specifically, for angles of incidence greater than the angle of RMS slope $\theta_K = \pi/2 - \tan^{-1}(\sigma\sqrt{2}/T)$ the energy scattered is significantly overestimated and the scattered intensity cannot be calculated acceptably without shadowing functions [35]. Note that θ_K and ξ_K are only applicable to surfaces with a Gaussian height distribution and a Gaussian correlation function.

4. Surface roughness estimation

The statistical parameters necessary for characterizing rough surfaces are the RMS roughness σ , the correlation length T , and the RMS slope m . In this section, we present some techniques for estimating these parameters. For

surfaces with a Gaussian correlation function, if two of these quantities are known, then the third one may be obtained using the formula $m = \sigma\sqrt{2}/T$. Note that the quantity $\sigma_g = \sigma\sqrt{2}/T$ has also been referred to as the RMS gradient [9]. However, for very-rough surfaces we can only estimate the ratio of the RMS roughness to the correlation length σ/T which is used in Eqs. (4)–(5) and (7)–(10). The estimated ratio σ/T allows us to compute the angle of RMS slope θ_K of Caron et al. [35]. Therefore, we consider only two groups of surfaces. These are dielectrics with small roughness ($\sigma \ll \lambda$) or large roughness ($\sigma \gg \lambda$). The parameter estimation methods described here are based on the minimum number of measurements required. Of course, if a larger number of measurements are available then least-square fitting techniques can be used as an alternative.

4.1. Surfaces with small roughness

The first case that we consider is to estimate σ and T for slightly rough dielectric surfaces.

4.1.1. Estimating RMS roughness σ

When the surface is smooth enough to produce a well-defined specular beam, the RMS roughness can be determined from the specular reflectance [1,17,20,32,36]. When the surface is under off-normal illumination (Fig. 5(a)), we can use the model developed by Torrance [23] for the specular direction to compute the specular reflectance as a function of the incidence angle ($\theta_i = \theta_s = \theta$):

$$R_{spec} = R_0 \exp[-g(\theta, \theta)] = R_0 \exp[-(4\pi\sigma \cos \theta / \lambda)^2], \quad (12)$$

where R_0 is the specular reflectance of a perfectly smooth surface of the same material. Note that the term R_0 is identical to the term ρ_0^2 used in Eq. (1). We determine an experimental value for the relative pixel brightness R_{spec} by measuring both the total peak pixel brightness \tilde{E}_{tot} at the center of the specular highlight and the average diffuse pixel brightness \tilde{E}_{dif} in the neighborhood of the specular lobe. The relative pixel brightness can then be approximated using the formula $R_{spec} = 1 - (\tilde{E}_{dif}/\tilde{E}_{tot})$. Here, the mean wavelength λ of the light source is assumed to be known. Hence, the RMS roughness is

$$\sigma = (\lambda/4\pi \cos \theta) [\ln(R_0/R_{spec})]^{1/2}. \quad (13)$$

4.1.2. Estimating correlation length T

With a value of the RMS roughness σ available, then we can proceed to measure the correlation length T . To do this we measure two values of pixel brightness $E_d(\theta_1, \pi, 0, 0)$ and $E_d(\theta_2, \pi, 0, 0)$ at a single point on the surface for two different angles of incidence, i.e. $\theta_i = \theta_1$ and $\theta_i = \theta_2$ (Fig. 5(b)) when the planar surface is perpendicular to \vec{V} for both measurements, i.e. $\theta_s = \phi_s = 0$. The pixel brightness measurements are averaged over a neighborhood so that the effects of rough surface texture are smoothed away. Although the use of two different wavelengths is also possible, here we use

only one wavelength λ . Under such illumination conditions and from Section 2 we can write $F(\theta_i, 0, 0) = 1/\cos(\theta_i)$, $v_{xy}(\theta_i, 0, 0) = (2\pi/\lambda) \sin(\theta_i)$, $v_z(\theta_i, 0) = (2\pi/\lambda)[1 + \cos(\theta_i)]$, and $g(\theta_i, 0) = \sigma^2 v_z^2(\theta_i, 0)$. Using Eq. (3), the ratio is

$$\begin{aligned} \frac{E_d(\theta_i=\theta_1, \phi_i=\pi, \theta_s=0, \phi_s=0)}{E_d(\theta_i=\theta_2, \phi_i=\pi, \theta_s=0, \phi_s=0)} &= \frac{g(\theta_1, 0)F^2(\theta_1, 0, 0)}{g(\theta_2, 0)F^2(\theta_2, 0, 0)} \\ &\times \exp\{g(\theta_2, 0) - g(\theta_1, 0) + (T^2/4)[v_{xy}^2(\theta_2, 0, 0) \\ &- v_{xy}^2(\theta_1, 0, 0)]\}. \end{aligned} \quad (14)$$

Since all of the parameters appearing in the equation except T are known, we can estimate the correlation length T using the equation

$$T = 2 \left[\frac{g(\theta_1, 0) - g(\theta_2, 0) + \ln \zeta}{v_{xy}^2(\theta_2, 0, 0) - v_{xy}^2(\theta_1, 0, 0)} \right]^{1/2}, \quad (15)$$

where $\zeta = [g(\theta_2, 0)F^2(\theta_2, 0, 0)E_d(\theta_1, \pi, 0, 0)]/[g(\theta_1, 0)F^2(\theta_1, 0, 0)E_d(\theta_2, \pi, 0, 0)]$.

4.2. Surfaces with large roughness

For very-rough dielectrics, the B–K model may also be used to estimate the ratio σ/T from a pair of pixel brightness measurements (Fig. 5(b)). From Eq. (4) for surfaces with a Gaussian correlation function ($T = T_G$), the ratio is

$$\begin{aligned} \frac{E_d(\theta_i=\theta_1, \phi_i=\pi, \theta_s=0, \phi_s=0)}{E_d(\theta_i=\theta_2, \phi_i=\pi, \theta_s=0, \phi_s=0)} &= \frac{F^2(\theta_1, 0, 0)v_z^2(\theta_2, 0)}{F^2(\theta_2, 0, 0)v_z^2(\theta_1, 0)} \\ &\times \exp \left\{ \frac{T_G^2}{4\sigma^2} \left[\frac{v_{xy}^2(\theta_2, 0, 0)}{v_z^2(\theta_2, 0)} - \frac{v_{xy}^2(\theta_1, 0, 0)}{v_z^2(\theta_1, 0)} \right] \right\}. \end{aligned} \quad (16)$$

Hence, the ratio σ/T_G , which is a measure of the surface slope, is estimated using the equation

$$\frac{\sigma}{T_G} = \frac{1}{2} \left\{ \frac{1}{\ln \kappa} \left[\frac{v_{xy}^2(\theta_2, 0, 0)}{v_z^2(\theta_2, 0)} - \frac{v_{xy}^2(\theta_1, 0, 0)}{v_z^2(\theta_1, 0)} \right] \right\}^{1/2}, \quad (17)$$

where $\kappa = [F^2(\theta_2, 0, 0)v_z^2(\theta_1, 0)E_d(\theta_1, \pi, 0, 0)]/[F^2(\theta_1, 0, 0)v_z^2(\theta_2, 0)E_d(\theta_2, \pi, 0, 0)]$. From the estimated ratio σ/T_G , we can easily compute the two quantities θ_K and ξ_K as described in Section 3.5. The technique used above to estimate the surface slope parameter may also be applied to surfaces with an exponential correlation function ($T = T_E$) using Eq. (5). Here, the pixel brightness ratio is

$$\begin{aligned} \frac{E_d(\theta_i=\theta_1, \phi_i=\pi, \theta_s=0, \phi_s=0)}{E_d(\theta_i=\theta_2, \phi_i=\pi, \theta_s=0, \phi_s=0)} &= \frac{F^2(\theta_1, 0, 0)v_z^2(\theta_2, 0)}{F^2(\theta_2, 0, 0)v_z^2(\theta_1, 0)} \\ &\times \left\{ \frac{1 + (T_E^2/\sigma^2)[v_{xy}^2(\theta_2, 0, 0)/v_z^2(\theta_2, 0)]}{1 + (T_E^2/\sigma^2)[v_{xy}^2(\theta_1, 0, 0)/v_z^2(\theta_1, 0)]} \right\}^{3/2}. \end{aligned} \quad (18)$$

Hence, the ratio σ/T_E is estimated using the equation

$$\frac{\sigma}{T_E} = \left\{ \frac{1}{\kappa^{2/3} - 1} \left[\frac{v_{xy}^2(\theta_2, 0, 0)}{v_z^2(\theta_2, 0)} - (\kappa^{2/3}) \frac{v_{xy}^2(\theta_1, 0, 0)}{v_z^2(\theta_1, 0)} \right] \right\}^{1/2}, \quad (19)$$

where κ is identical to that given above. In general, we do not restrict ourselves to small angles of incidence. Hence, we should use the F factor of V–H ($F = F_{VH}$) in Eqs. (15), (17), and (19) to compute the corresponding estimates.

5. Experimental results

Our experimental evaluation of the physics-based models for rough surface reflectance is divided into three parts. We commence in Section 5.1 by showing how the methods developed in Section 4 can be used to estimate the physical roughness parameters for a variety of different materials. In Section 5.2 we show the results of fitting the original and the modified B–K model to pixel brightness data for cylindrical objects. In Section 5.3 we compare the BRDF data from the CURET database [26] with the predictions from several variants of the B–K model.

The experimental facilities at our disposal are relatively rudimentary. The images used in our roughness estimation experiments have been captured using an Olympus Camedia E-10 camera. Each surface has been imaged under controlled lighting conditions in a darkroom. The geometries of the experimental setups are shown in Fig. 5. The objects have been illuminated using a single collimated tungsten light source with parallel beams whose mean wavelength is approximately 555 nm. The bulb was a 24 V, 200 W, Thorn Atlas A1/252 projector lamp with a coiled filament emitting white light. The light source was placed 2 m away from the objects and collimated using a cylindrical tube 0.5 m long and with diameter 0.12 m. The distance between the camera and the objects was 1.5 m. As a result the light source is not a perfect point source, however the central part of each image was used to achieve the best approximation. The camera had a zoom auto focus lens with a focal length that varied between 9 and 36 mm, and 2240 (horizontal) \times 1680 (vertical) pixel CCD array. Apertures between $f/2$ and $f/11$ were

available, but $f/3.2$ was used for the measurements. The camera direction \vec{V} is aligned with the z -axis and the light-source direction \vec{L} is recorded when capturing the images. To experiment under $\vec{L} \approx \vec{V}$ conditions, the source and camera are slightly displaced in the vertical plane.

Although scattering and specular reflectance measurements were made with the digital camera, no independent topographic measurements were made on any of the samples. Therefore, none of the actual RMS topographic roughnesses or correlation lengths were known. Furthermore, we cannot confirm that all the samples studied fit well to the assumptions of the theories. Hence, the relative roughness estimates are not claimed to be as accurate as the values obtained using advanced tactile sensors such as profilometers.

5.1. Roughness estimation for plane samples

We commence by showing how the B–K theory can be used to estimate surface roughness for slightly rough dielectric surfaces. Here, we study a porcelain plate, a white plastic plate and glossy paper. For each of these surfaces we capture one image under off-normal illumination and in the specular direction (Fig. 5(a)). Here $\theta_i = \theta_s = 14^\circ$. These images are shown in Fig. 6. We have enhanced the contrast of the white plastic image by 80%, since the original image contained little brightness structure and was difficult to interpret. Here, we use the B–K model for the specular direction to find the surface roughness σ (Eq. (13)). We also estimate the correlation length T using the technique outlined in Section 4.1.2 (Eq. (15)).

Here, we capture two images illuminated from different directions, $\theta_i = 30^\circ$ and 45° and use these to make estimates of $E_d(\theta_i = 30^\circ, 0, 0, 0)$ and $E_d(\theta_i = 45^\circ, 0, 0, 0)$ at corresponding image locations (Fig. 5(b)). We have not shown these images here since there is little visible difference between them. The main reason for this is that for these surfaces the irregularities and topographic features are not visible by naked eye. We present the resulting estimates of σ , T , and also their ratio σ/T in Table 1. When both the distribution of surface height deviations and the correlation function is assumed to be Gaussian, then a simple method to evaluate the roughness estimates is as follows. If the surface is slightly rough, then the condition $\sigma \ll T$ holds, while

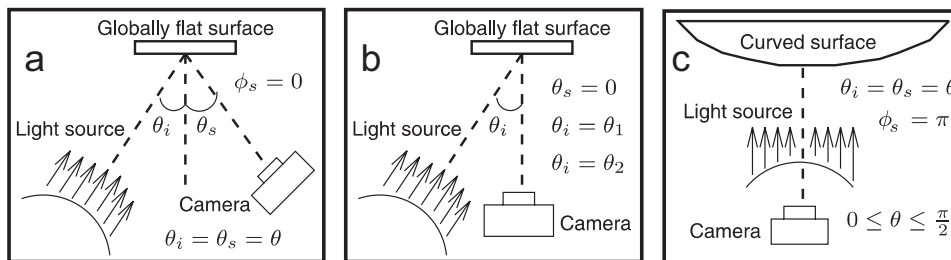


Fig. 5. Experimental setup: (a) non-normal incidence for measuring specular reflection of plane surfaces, (b) non-normal incidence illumination and viewing direction on surface normal for estimating surface parameters, and (c) retroscattering configuration for reflectance modeling of cylindrical surfaces and three-dimensional objects.

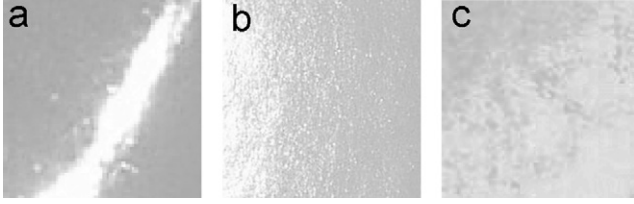


Fig. 6. Images of small parts of the three slightly rough surfaces illuminated at 14° and viewed in the specular direction: (a) porcelain plate (2.1×2.1 cm), (b) glossy paper (2.5×2.5 cm), and (c) plastic plate (2.2×2.2 cm). The sizes of the masked areas on the samples are given in parentheses.

when the surface is moderately rough then $\sigma \approx T$, and finally, when the surface is very rough then $\sigma \gg T$. Looking at the estimates for our slightly rough surfaces in Table 1, it is clear that the condition $\sigma \ll T$ holds. This means that these estimates are sensible for the corresponding surfaces.

Next, we present results for very-rough dielectric surfaces. The samples used in our study are stone tiles, textured wall papers, sandpapers, and a wooden cube. For each of these surfaces, we capture two images under two different incidence angles (Fig. 5(b)), i.e. $\theta_i = 30^\circ$ and 45° ($F = F_{VH}$). Images of each pair are very similar and the differences are not visible by naked eye. Hence in Fig. 7 we only show the images taken at $\theta_i = 30^\circ$. For these surfaces we use the method explained in Section 4.2 using both variants of the modified B–K model (Eqs. (17) and (19)) to find the corresponding ratios σ/T_G and σ/T_E . The results are presented in Table 2. For surfaces with an identical assumed height distribution function (Gaussian) and two different correlation functions, i.e. the Gaussian and the exponential, we expect to find two different values of σ/T for each surface. The reason is that while σ is unaffected by the changes of correlation function, the different correlation functions will result in different estimates for the correlation length (T_G and T_E). To gauge the validity of the model, for very-rough surfaces with a Gaussian correlation function we can also

compute the angle of RMS slope θ_K , which gives an upper limit for the valid incidence angles, and the energy conservation rate ξ_K , which measures the fraction of the energy that is not absorbed by the surface.

It is important to note that roughness estimates are not necessarily consistent across multiple samples of the same material, because it is the surface irregularities that play the main role in deciding which category of roughness the surface belongs to. Hence, the roughness estimation methods outlined in this paper may be used to classify surfaces with similar roughness not with similar material. For instance, consider an artistic statue made of white marble. One experiment would be to classify different parts of the statue as exhibiting roughness measures falling in one of the three broad categories, i.e. slightly rough, moderately rough and very rough. Obviously, different parts of the statue may fall into different categories. A more detailed experiment is to compare surface patches falling into an identical category using their corresponding roughness estimates. Note that if different materials are used in different parts of the statue we may still find some parts falling into an identical category exhibiting very close roughness estimates.

5.2. Models against radiance data from rough cylinders

With the roughness parameters available, we can compare the predictions of the B–K model with measured pixel brightness data for curved objects. In order to simplify the comparison, we work with cylindrical objects since we can estimate the incidence angles using simple geometry. Hence, we have constructed cylinders using the two samples of sandpaper (types 1 and 2) previously used to estimate the values of σ/T (Table 2). We illuminate each cylinder so that $\vec{L} \approx \vec{V}$ (Fig. 5(c)). The B–K model applicable to this case is summarized by Eqs. (7)–(10). We use the estimated values of σ/T for the samples of sandpaper to compare the predictions of the model with the data for the cylinders in the following way.

Table 1
Results for the slightly rough dielectric surfaces shown in Fig. 6

Surface type	R_{spec}	σ (μm)	E_1/E_2	T (μm)	σ/T
Glossy paper	0.014	0.094	1.043	0.195	0.482
Porcelain plate	0.003	0.109	1.047	0.256	0.424
Plastic plate	0.002	0.115	1.032	0.276	0.416

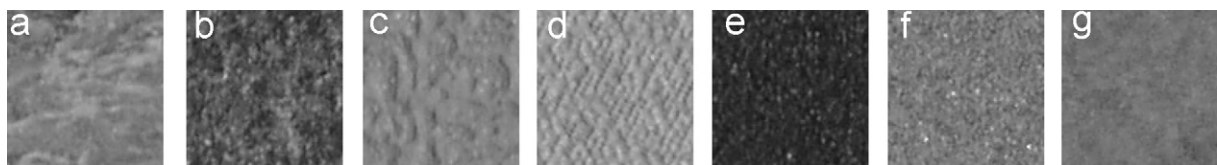


Fig. 7. Images of (a) and (b) stone tiles, (c) and (d) textured wall papers, (e) and (f) sandpapers, and (g) one side of a wooden cube ($\theta_i = 30^\circ$). The sizes of the masked objects are 2.1×2.1 cm.

Table 2

Results for the very-rough dielectric surfaces shown in Fig. 7

Surface type	E_1/E_2	σ/T_G	$\theta_K(^{\circ})$	$\zeta_K(\%)$	σ/T_E
Stone tile 1	1.056	0.9126	38	25.9	2.2080
Stone tile 2	1.141	0.4833	56	65.7	1.1315
Wall paper 1	1.077	0.7104	45	39.1	1.7050
Wall paper 2	1.070	0.7654	43	34.7	1.8420
Sandpaper 1	1.091	0.6332	48	46.4	1.5113
Sandpaper 2	1.088	0.6483	47	44.8	1.5494
Wooden cube	1.079	0.6964	45	40.3	1.6697

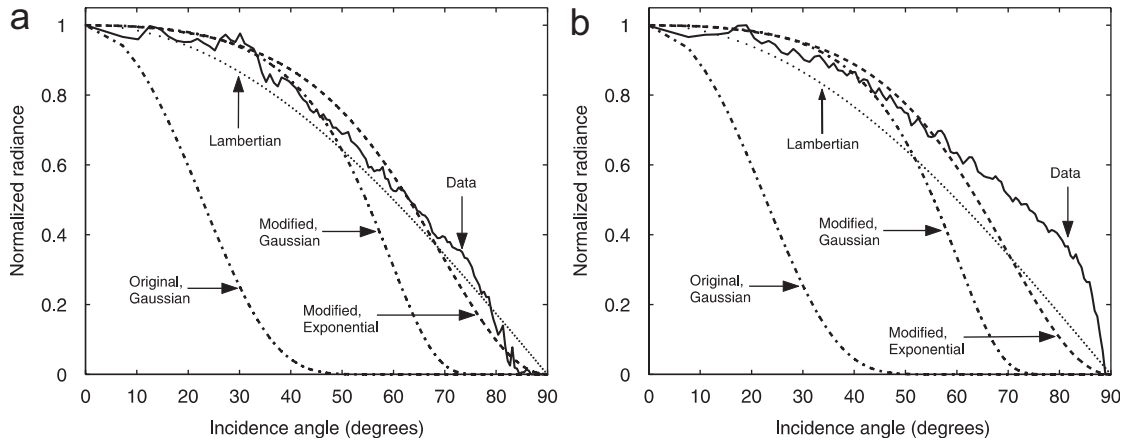


Fig. 8. Normalized radiance (solid) for sandpaper cylinders type 1 (a) and type 2 (b) versus incidence angle compared to three variants of the B–K model and Lambertian model.

Across a horizontal line, perpendicular to the axis of each cylinder, we compute the mean brightness at each point (on the right-hand half-cylinders) by averaging the brightness values over the vertical neighbors. The mean-brightness values computed in this way are shown as a function of the incidence angles (computed from the known cylindrical geometry) in Figs. 8(a) and (b) as solid curves. In this figure, subfigures (a) and (b) are for the sandpapers of type 1 and 2, respectively. Here, we show the Lambertian model (dotted curve), the original B–K model with a Gaussian correlation function (Eq. (7), dash-dot curve), the V–H modified B–K model with both a Gaussian (Eq. (9), dash-dot curve), and an exponential (Eq. (10), dashed curve) correlation function.

In both plots, only for $\theta_i < 10^\circ$, the data are close to the predictions of the original B–K model. However, and as expected, they deviate significantly from this model as the incidence angle increases. In subfigure (b), for $\theta_i < 45^\circ$ the data curve fits well to both variants of the modified B–K model, while it deviates significantly from the Lambertian model. In subfigure (a), on the other hand, there is good agreement between the data and both variants of the modified B–K model at most incidence angles. However, in both plots, for large incidence angles in subfigure (a), the modified B–K model with an exponential correlation function is much closer to the data than the remaining models. This supports the claims in Refs. [8,9] that the exponential correlation function gives

a better fit to measured surface data. From these plots, it is also clear that the V–H modification results in good agreement between the modified B–K model and the real-world data. As noted earlier the failure of the models at large angles is attributable to multiple scattering effects [33] and, as noted by Caron et al. [35], can be characterized using the energy conservation rate, ζ_K , and the upper limit for the incidence angles, θ_K . For the two samples of sandpaper used here, the energy conservation rates $\zeta_K = 46.40\%$ and 44.83% (Table 2) suggest the possibility that the scattered energy may have been misestimated by as much as 50% when the B–K theory is used. Moreover, $\theta_K = 48.16^\circ$ and 47.48° (Table 2) are very close to the incidence angles given by Fig. 8 above which the B–K theory is expected to fail. The angle at which the curve corresponding to the modified B–K model (with a Gaussian correlation function) moves away from the data curve is about 46° in Fig. 8(a) and 44° in Fig. 8(b). One possible reason for disagreements between the models and the data at large angles of incidence may also be caused by the fact that the surfaces under study do not satisfy the assumptions on which the models are based. For instance, since the particles on surface of the sandpaper are quite large, they are unlikely to have a Gaussian height distribution. To conclude from these experiments, we found that for dielectric surfaces with different scales of roughness, it is the modified B–K model which results in reasonable

predictions of brightness for most angles of incidence and reflectance. Also, for the very-rough surfaces, the modified B–K model with an exponential correlation function gives the best agreement with the real-world data.

5.3. Models against radiance data from BRDF measurements

In this section, we compare the predictions of some variants of the B–K model with the BRDF data for several rough surface samples provided in the CURET database [26,28]. Here, the data was collected with the following setup. For each of the samples studied, the BRDF was measured by recording images of the sample under 205 different combinations of viewing and illumination directions. The recorded images were radiometrically calibrated to obtain the radiance and BRDF from the pixel brightness values. Gain and offset values were used to transform the average pixel brightness values into radiance measurements using the formula $\text{radiance} = \text{gain} * \text{pixel} + \text{offset}$. Here, the radiance has units of $\text{W}/\text{sr m}^2$ and is summed over the wavelength range 380–780 nm. The pixel brightness is taken as the average of the R/G/B brightness values. The brightness of the lamp is also estimated so that BRDF can be obtained from the radiance. This was done by recording the radiance from a Kodak 18% gray card using a photometer. During the experiments three lamps were used. However, a single lamp was used to experiment with each surface sample.

We also investigate the predictions of a variant of the O–N model [13] which includes interreflections, i.e. the effects of adjacent surface elements on each other when reflecting the incident light (as discussed in geometrical optics). For the O–N model, we use the parameters which have been estimated and tabulated in the database for each sample. As an empirical reflectance model, we choose the Lafortune et al. (LFTG) model [37] which is an improved version of the Phong model. We only consider the diffuse reflectance component for which the exponent n_d is the single parameter controlling the fit of the model to the data. To compare the fit of the models to the data, one method is to test many values in some possible ranges for all model parameters. The parameter value giving the lowest total error when fitting to the data would result in the best fit. Another method is to estimate the value for each model parameter directly from few data measurements. Obviously, the latter method is less precise but much quicker and more practical especially when small number of data measurements are available for a surface. For the LFTG model we find the value of n_d using the former method, i.e. using a least-square method which involves exhaustively searching for a value in the interval [0.1, 20.0] which gives the best fit of the model to the radiance data. For the B–K model, on the other hand, we use the latter method, and estimate the parameters using the method outlined in Section 4.2. This requires only two radiance measurements at two different off-normal incidence angles and for both measurements the

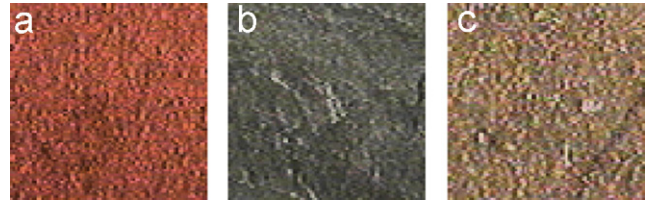


Fig. 9. CURET database: images of (a) quarry tile (25), (b) slate b (34), and (c) brick b (41).

light must be normally incident i.e. $\theta_s = 0$ and $\phi_s = 0$. The CURET database provides BRDF measurements at 205 different illumination configurations for each surface sample. Hence, each data (measurement) index number (between 1 and 255) corresponds to an individual setting of the four angles θ_i , ϕ_i , θ_s , and ϕ_s . Fortunately, there are measurements in the tables that satisfy these illumination conditions. These are the ones with measurement index numbers 81 and 112 where $\theta_i = \theta_1 = 45.5^\circ$ and $\theta_i = \theta_2 = 67.5^\circ$, respectively. To compare theory with experiment, we convert the measured BRDF $f(\theta_i, \phi_i, \theta_s, \phi_s)$ in the tables into the radiance $\mathcal{L}_o(\theta_s, \phi_s)$ estimates which are equivalent to the irradiance estimates $E(\theta_i, \phi_i, \theta_s, \phi_s)$ (as described in Section 2). This is a straightforward task since the incidence angle θ_i and the radiance of the light source \mathcal{L}_i which is constant for each surface sample are tabulated, and hence $\mathcal{L}_o(\theta_i, \phi_i, \theta_s, \phi_s) \propto f(\theta_i, \phi_i, \theta_s, \phi_s) \mathcal{L}_i \cos(\theta_i) d\omega$ or equally $E(\theta_i, \phi_i, \theta_s, \phi_s) \propto f(\theta_i, \phi_i, \theta_s, \phi_s) \cos(\theta_i)$. The variants of the B–K model studied here are the original B–K model ($F = F_{Beck}$) and the V–H modification ($F = F_{VH}$). We focus on the model variants that apply to very-rough surfaces, and where the correlation functions are either Gaussian or exponential. The samples studied (with their corresponding numbers in the database) are quarry tile (25), slate b (34) and brick b (41). We show the images of these surface samples in Fig. 9. In their study of these data, Koenderink et al. [27] have noted that the observations are relatively sparse, and hence their visualization over the four angular variables is not a straightforward task. To overcome these problems, in Fig. 10 we plot the normalized radiance data versus the data index ordered according to increasing radiance. We have sorted the BRDF measurement indices in order of increasing radiance so that we can compare them with different reflectance models more conveniently. This method of sorting results in slowly varying data curves, but rather irregular model curves. The data index can also be sorted according to the model radiance values. However, we choose the former method since it allows us to easily contrast the model predictions against a fixed representation of the measured data. In Table 3 we list the surface parameters estimated from the BRDF measurements. The image brightness ratios needed to estimate the parameters are related to the BRDF measurements using the formula $(E_1/E_2) = (E_d(\theta_1, \pi, 0, 0)/E_d(\theta_2, \pi, 0, 0)) = f(\theta_1, \pi, 0, 0) \cos(\theta_1)/f(\theta_2, \pi, 0, 0) \cos(\theta_2)$.

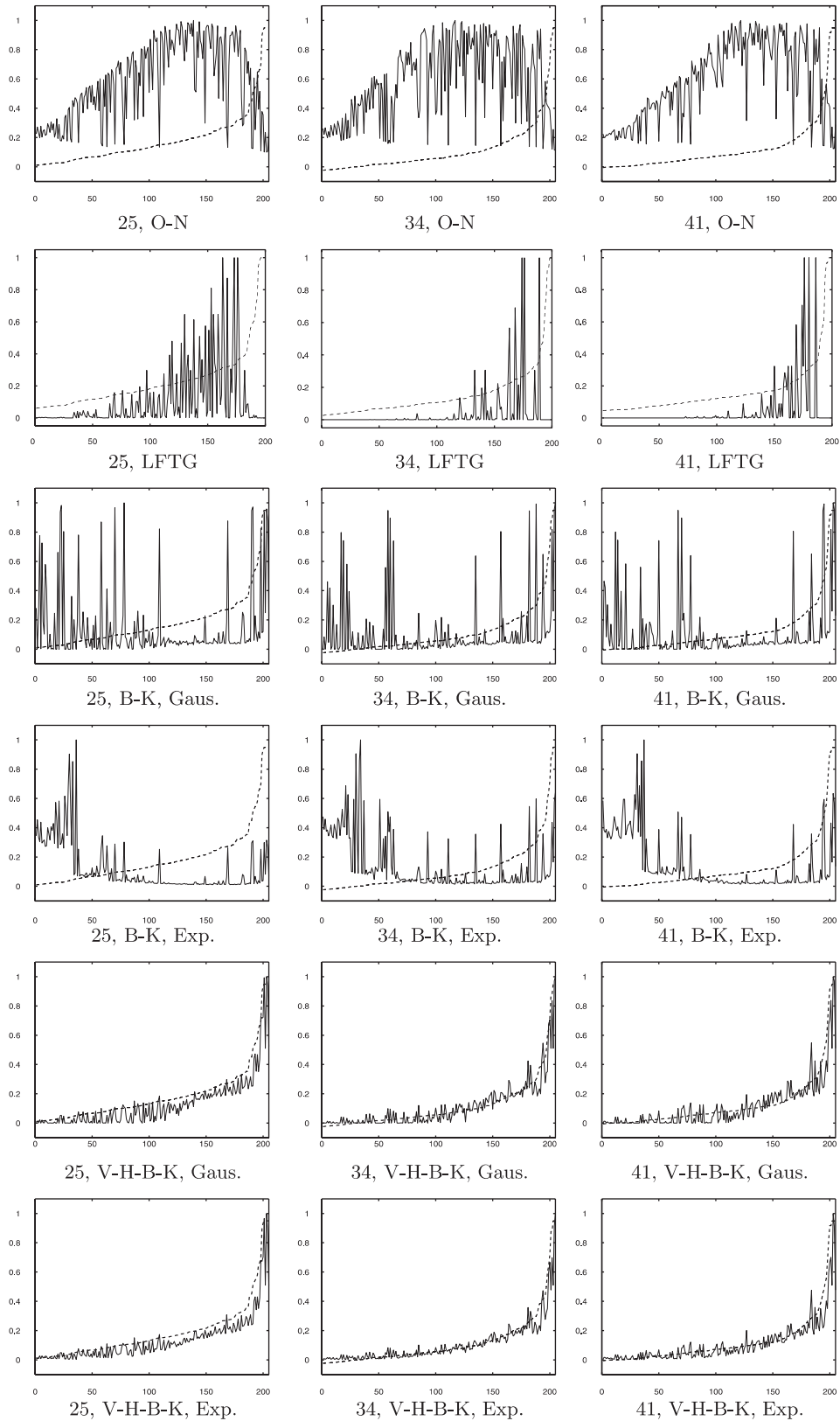


Fig. 10. Normalized radiance for samples 25, 34, and 41 calculated using the Oren-Nayar (O-N) model, the Lafortune et al. (LFTG) model, the original B-K model (B-K), and the Vernold-Harvey (V-H-B-K) modification, with a Gaussian (Gaus.) or an exponential (Exp.) correlation function. The identification is given under each graph.

Table 3
Model parameter estimates for the surface samples shown in Fig. 9

Surface sample (no.)	E_1/E_2	σ/T_G	σ/T_E	$\sigma_{ON}(\text{rad})$	ρ_{ON}	$n_d(\text{LFTG})$
Quarry tile (25)	1.880176	0.3957	0.7982	0.3606	0.1060	3.50
Slate b (34)	2.194214	0.3403	0.6284	0.3096	0.0685	9.50
Brick b (41)	2.189937	0.3409	0.6302	0.2760	0.0577	9.06

Table 4
Mean square errors for the models studied and the surface samples shown in Fig. 9

Surface sample (no.)	O–N	LFTG	B–K(G)	B–K(E)	V–H–B–K(G)	V–H–B–K(E)
Quarry tile (25)	46.9	14.95	17.175	19.712	3.150	2.971
Slate b (34)	57.5	9.55	10.827	14.834	1.413	1.421
Brick b (41)	57.7	10.86	11.347	15.369	2.012	2.052

It is clear that our irradiance ratios are identical to radiance ratios. Here, we have used irradiance ratios since they are consistent with the notation used earlier in the corresponding equations (Eqs. (16)–(19)).

Table 3 lists the surface slope parameters estimated using the modified B–K model with the Gaussian (σ/T_G) and exponential (σ/T_E) correlation functions (as described in Section 4.2). We also list the values of the two parameters of the O–N model [13] which are tabulated in the CURET database. These are the surface albedo ρ_{ON} which represents the surface reflectivity ratio and the angular slope parameter σ_{ON} which measures the distribution of cavity wall slope angles, and is hence measured in degrees or radians (rad) [13].

Once the estimates of surface slope parameter σ/T are obtained, then we can compare the radiance predictions of the B–K model variants with the values extracted from the BRDF measurements. In Fig. 10, the plots in each row correspond to a different surface sample. Here, we plot the normalized radiance versus the data index ordered by increasing radiance. In each plot the solid curve corresponds to the model prediction while the dashed curve corresponds to the measurements extracted from the tabulated BRDF values. In Fig. 10, the top row shows the results obtained using the O–N model, the second row those obtained using the LFTG model, the third and fourth rows those obtained using the original B–K model, and the fifth and the bottom rows those obtained using the V–H modification. Note that, the third and fifth rows are for Gaussian correlation function, and the fourth and the bottom rows are for the exponential correlation function.

To evaluate the quality of the fit of the models to the data, we have computed the mean square error (MSE) between the predicted normalized radiance and the normalized radiance data derived from the tabulated BRDF measurements in the CURET database. The results are shown in Table 4. The modified B–K model gives MSE values that are always lower than those obtained with the original model, and in all cases (slate b, brick b, quarry tile) an order of magnitude lower.

For the modified B–K model it is difficult to distinguish between the exponential and Gaussian correlation functions on the basis of MSE. For the original B–K model, the Gaussian correlation function always gives a slightly lower MSE than the exponential one. The O–N model results in an MSE which is always larger than both the original and modified B–K models. The LFTG model results in MSE which is lower than that obtained by the O–N model and higher than that obtained with the V–H modification for the samples studied. These conclusions are supported by the plots shown in Fig. 10. Here, for all surface samples studied, the modified B–K model gives the qualitatively best fit. However, here it is the exponential correlation function that seems to give a better qualitative fit to the data than the Gaussian correlation function. Moreover, none of these samples is fitted well by the O–N model.

6. Conclusions

The main contribution in this paper has been to explore the use of a family of reflectance models from physical optics for rough surface analysis tasks in vision. We have investigated the Beckmann–Kirchhoff (B–K) theory [10] and its variants by Vernold and Harvey [22], and by Caron et al. [35]. We have provided a review of different variants of the reflectance model and have commented on their domain of applicability. Using the models, we have considered how they may be applied to a number of different surface analysis tasks.

The first problem addressed was that of developing simple methods for estimating the physical parameters of rough surfaces using just a light source and a digital camera. For slightly rough surfaces, both the RMS roughness and the correlation length are estimated. For very-rough surfaces, we have estimated the ratio of the RMS roughness to the correlation length. These estimated parameters allow the B–K model to be fitted to real-world data. While the modified B–K model of V–H fits well to the data, the original B–K model only fits well to the data for small incidence angles.

The results are encouraging, since they indicate that wave scatter theory can be used in conjunction with simple experimental instruments, i.e. the visible light and a digital camera, to make surface roughness measurements.

Finally, we have shown that the modified B–K model gives an accurate account of BRDF measurements from the CURET database [26] for a variety of rough surfaces. The model outperforms the alternatives studied, specifically the empirical reflectance model of LFTG [37]. Hence, we believe that the proposed techniques have significant potential in computer vision for texture model acquisition and realistic reflectance modeling.

References

- [1] R.L. Cook, K.E. Torrance, A reflection model for computer graphics, *ACM Trans. Graphics* 1 (1) (1982) 7–24.
- [2] B. van Ginneken, M. Stavridi, J.J. Koenderink, Diffuse and specular reflectance from rough surfaces, *Appl. Opt.* 37 (1) (1998) 130–139.
- [3] T. Leung, J. Malik, Representing and recognizing the visual appearance of materials using three-dimensional textures, *Int. J. Comput. Vision* 43 (1) (2001) 29–44.
- [4] M. Chantler, M. Schmidt, M. Petrou, G. McGunnigle, The effect of illuminant rotation on texture filters: Lissajous's ellipses, in: *European Conference on Computer Vision*, Copenhagen, 2002, pp. 289–303.
- [5] Y. Sun, Self shadowing and local illumination of randomly rough surfaces, in: *Proceedings of the Computer Vision and Pattern Recognition (CVPR) 2004*, Washington, DC, 2004, pp. 158–165.
- [6] B.G. Smith, Geometrical shadowing of a random rough surface, *IEEE Trans. Antennas Propag.* AP-15 (5) (1967) 668–671.
- [7] R.A. Brockelman, T. Hagfors, Note on the effect of shadowing on the backscattering of waves from a random rough surface, *IEEE Trans. Antennas Propag.* AP-14 (5) (1965) 621–626.
- [8] J.M. Bennett, L. Mattsson, *Introduction to Surface Roughness and Scattering*, second ed., Optical Society of America, Washington, DC, 1999.
- [9] J.A. Ogilvy, *Theory of Wave Scattering from Random Rough Surfaces*, Adam Hilger, Bristol, 1991.
- [10] P. Beckmann, A. Spizzichino, *The Scattering of Electromagnetic Waves from Rough Surfaces*, Pergamon, New York, 1963.
- [11] K.E. Torrance, E.M. Sparrow, Theory for off-specular reflection from roughened surfaces, *J. Opt. Soc. Am.* 57 (9) (1967) 1105–1114.
- [12] S.K. Nayar, K. Ikeuchi, T. Kanade, Surface reflection: physical and geometrical perspectives, *IEEE Trans. Pattern Anal. Mach. Intell.* 13 (7) (1991) 611–634.
- [13] M. Oren, S.K. Nayar, Generalization of the Lambertian model and implications for machine vision, *Int. J. Comput. Vision* 14 (3) (1995) 227–251.
- [14] L.B. Wolff, S.K. Nayar, M. Oren, Improved diffuse reflection models for computer vision, *Int. J. Comput. Vision* 30 (1) (1998) 55–71.
- [15] J.M. Elson, H.E. Bennett, J.M. Bennett, Scattering from optical surfaces, *Appl. Opt. Opt. Eng.* VII (1979) 191–244.
- [16] P. Beckmann, Scattering of light by rough surfaces, in: E. Wolf (Ed.), *Progress in Optics*, vol. VI, 1967, pp. 55–69.
- [17] H.E. Bennett, J.O. Porteus, Relation between surface roughness and specular reflectance at normal incidence, *J. Opt. Soc. Am.* 51 (2) (1961) 123–129.
- [18] H. Davies, The reflection of electromagnetic waves from a rough surface, *Proc. IEEE Part IV* 101 (1954) 209–214.
- [19] C.A. Depew, R.D. Weir, Surface roughness determination by the measurement of reflectance, *Appl. Opt.* 10 (4) (1971) 969–970.
- [20] P.J. Chandley, Surface roughness measurements from coherent light scattering, *Opt. Quantum Electron.* 8 (1976) 323–327.
- [21] J.E. Harvey, C.L. Vernold, A. Krywonos, P.L. Thompson, Diffracted radiance: a fundamental quantity in a non-paraxial scalar diffraction theory, *Appl. Opt.* 38 (1999) 6469–6481.
- [22] C.L. Vernold, J.E. Harvey, A modified Beckmann–Kirchhoff scattering theory for non-paraxial angles, *Scattering and surface roughness II*, *Proc. SPIE* 3426 (1998) 51–56.
- [23] K.E. Torrance, Monochromatic directional distribution of reflected thermal radiation from roughened dielectric surfaces, M.S. Thesis, University of Minnesota, 1964.
- [24] X.D. He, K.E. Torrance, F.X. Sillion, D.P. Greenberg, A comprehensive physical model for light reflection, *ACM Comput. Graphics* 25 (1991) 175–186.
- [25] B.K.H. Horn, *Robot Vision*, MIT Press, Cambridge, MA, 1986.
- [26] CURET database. (www.cs.columbia.edu/CAVE/curet).
- [27] J.J. Koenderink, A.J. van Doorn, M. Stavridi, Bidirectional reflection distribution function expressed in terms of surface scattering modes, in: *European Conference on Computer Vision*, vol. 2, 1996, pp. 28–39.
- [28] K.J. Dana, S.K. Nayar, B. van Ginneken, J.J. Koenderink, Reflectance and texture of real-world surfaces, in: *Proceedings of the IEEE Computer Vision and Pattern Recognition*, 1997, pp. 151–157.
- [29] M. Nieto-Vesperinas, N. Garcia, A detailed study of the scattering of scalar waves from random rough surfaces, *Opt. Acta* 28 (12) (1981) 1651–1672.
- [30] M. Nieto-Vesperinas, Radiometry of rough surfaces, *Opt. Acta* 29 (7) (1982) 961–971.
- [31] D.H. Berman, J.S. Perkins, Exponential substitution for Kirchhoff scattering from Gaussian rough surfaces, *J. Acoust. Soc. Am.* 78 (1985) 1024–1028.
- [32] E. Marx, T.V. Vorburger, Direct and inverse problems for light scattered by rough surfaces, *Appl. Opt.* 29 (25) (1990) 3613–3626.
- [33] K.A. O'Donnell, E.R. Mendez, Experimental study of scattering from characterized random surfaces, *J. Opt. Soc. Am. A* 4 (7) (1987) 1194–1205.
- [34] H. Ragheb, E.R. Hancock, Surface radiance correction for shape-from-shading, *Pattern Recognition* 38 (10) (2005) 1574–1595.
- [35] J. Caron, J. Lafait, C. Andraud, Scalar Kirchhoff's model for light scattering from dielectric random rough surfaces, *Opt. Commun.* 207 (2002) 17–28.
- [36] D.E. Barrick, Rough surfaces scattering based on the specular point theory, *IEEE Trans. Antennas Propag.* 16 (1968) 449–454.
- [37] E.P.F. LaFortune, S. Foo, K.E. Torrance, D.P. Greenberg, Non-linear approximation of reflectance Functions, in: *Proceedings of SIGGRAPH*, 1997, pp. 117–126.

About the Author—HOSSEIN RAGHEB received his B.Sc. degree in Computer Engineering (Hardware) from the Isfahan University of Technology, Isfahan, Iran, in 1994 and his M.Sc. degree in Computer Engineering (Machine Intelligence and Robotics) from the University of Tehran, Tehran, Iran, in 1997. He received his Ph.D. degree in Computer Vision from the Department of Computer Science at the University of York, York, United Kingdom in 2004. In 2001, he won the “Young Scientist Award” for one of his papers presented at “9th International Conference on Computer Analysis of Images and Patterns (CAIP) held in Warsaw, Poland. He also successfully completed a post-doctoral research (physics-based reflectance models) at the university of York. Later, he started serving as a lecturer at the Bu-Ali Sina University, Hamedan, Iran. He is currently conducting research in Visual Surveillance at the Digital Imaging Research Centre (DIRC) of the Kingston University London, UK. So far, he has published some 35 papers in refereed conferences and journals.

About the Author—EDWIN R. HANCOCK studied physics as an undergraduate at the University of Durham and graduated with honours in 1977. He remained at Durham to complete a Ph.D. in the area of high energy physics in 1981. Following this he worked for 10 years as a researcher in the fields of high-energy nuclear physics and pattern recognition at the Rutherford-Appleton Laboratory (now the Central Research Laboratory of the Research

Councils). During this period, he also held adjunct teaching posts at the University of Surrey and the Open University. In 1991, he moved to the University of York as a lecturer in the Department of Computer Science. He was promoted to Senior Lecturer in 1997 and to Reader in 1998. In 1998, he was appointed to a Chair in Computer Vision.

Professor Hancock now leads a group of some 20 faculty, research staff and Ph.D. students working in the areas of computer vision and pattern recognition. His main research interests are in the use of optimisation and probabilistic methods for high and intermediate level vision. He is also interested in the methodology of structural and statistical pattern recognition. He is currently working on graph-matching, shape-from-X, image data-bases and statistical learning theory. His work has found applications in areas such as radar terrain analysis, seismic section analysis, remote sensing and medical imaging. Professor Hancock has published some 110 journal papers and 450 refereed conference publications. He was awarded the Pattern Recognition Society medal in 1991 and an outstanding paper award in 1997 by the journal *Pattern Recognition*. In 1998, he became a fellow of the International Association for Pattern Recognition.

Professor Hancock is Editor in Chief of the *IET Computer Vision Journal*, and has been a member of the Editorial Boards of the journals *IEEE Transactions on Pattern Analysis and Machine Intelligence* and *Pattern Recognition*. He has also been a guest editor for special editions of the journals *Image and Vision Computing* and *Pattern Recognition*. He has been on the programme committees for numerous national and international meetings. In 1997 with Marcello Pelillo, he established a new series of international meetings on energy minimisation methods in computer vision and pattern recognition.